Interactive Phenomena in Supersonic Jet Mixing Problems, Part II: Numerical Studies

Sanford M. Dash* and David E. Wolf†
Science Applications, Inc., Princeton, New Jersey

Applications of the numerical techniques discussed in Part I of this article are presented. Fundamental wave/shear-layer interaction calculations are performed exhibiting the waves produced by high-speed turbulent mixing processes and the interactions of an expansion fan and shock wave with a developing shear layer. Calculations for an underexpanded supersonic jet into a supersonic external stream at different velocity ratios are presented which delineate between weakly interactive and strongly interactive processes in the jet near field. Calculations for the multiple-cell shock structure of an underexpanded jet into still air exhibit the damping of wave intensities by the turbulence and compare quite favorably with available data.

Introduction

IN Part I of this article,[1] numerical modeling techniques were presented for solving the parabolized Navier-Stokes (PNS) equations for the analysis of interactive supersonic jet mixing problems. The present article describes a series of calculations performed which exhibit some of the interactive phenomena that occur and the ability of the modeling techniques developed to treat these phenomena. The first group of calculations performed isolates the fundamental wave/shear-layer interactions that occur in a supersonic mixing environment. Such interactions include the waves generated by turbulent dissipative processes in a simple supersonic shear layer, the interaction of an expansion fan with a developing shear layer, and the interaction of a shock wave with a developing shear layer. The interaction process involves the partial transmission and partial reflection of the wave in traversing the shear layer, the curvature of the wave front due to the strong flow rotationality, and the attenuation of the wave strength due to turbulent dissipation. The details of these processes are explored via inspection of the predicted pressure and temperature profiles in the interactive flow region.

The second group of calculations performed simulates the near-field flow structure of an underexpanded jet exhausting into a supersonic external stream. Two cases were performed, both having a nozzle exit plane static pressure ratio of 10/1. The first case simulates a Mach 3 jet exhausting into a Mach 3 external stream where a nominal velocity ratio of 2/1 prevails. Here, interactive processes in the near-field shear layer of the first shock cell are shown to be relatively weak and the pressure field could be adequately represented by an inviscid solution. Beyond the first cell, interactive processes become substantial and the inviscid and PNS solutions are shown to depart. The second case simulates a Mach 5 jet exhausting into a Mach 2 external stream with the nominal jet/external flow velocity ratio here about 7/1. Due to significantly faster mixing and larger Mach numbers in this case, turbulent dissipative effects are quite pronounced in the near-field shear layer and lead to substantial modifications of the pressure field in the first shock cell from that given by an inviscid prediction. This latter calculation typifies the strong near-field interactions that would occur in situations with significant afterburning occurring in the near-field shear layer of the jet exhaust.

The third group of calculations performed simulates the multiple-cell flow structure of an underexpanded jet exhausting into still air. The first case in this group simulates one of the experiments performed by Seiner and Norum[2,3] for which detailed flow data are available. Comparisons of the predicted and measured pressure variations in the jet, the jet sonic line variation, and jet turbulence levels are shown to be quite good. Further comparisons of this sort for Mach 1, 1.5, and 2 under- and overexpanded jets exhausting into still air are described in Ref. 4 and are, in general, quite favorable. The sensitivity of these calculations to the turbulence modeling is discussed in Ref. 5, where further calculations are presented exhibiting the influence of jet temperature and flight velocity on the jet shock structure. The second case in this group of calculations is analogous to the first with the exit pressure ratio boosted to generate Mach disks in the first several cells. The ability to routinely calculate the small embedded subsonic zones behind these disks is exhibited.

Wave/Shear-Layer Interactions

To illustrate some of the fundamental interactive phenomena that can occur in the near-field jet shear layer, a series of calculations were performed for a supersonic shear layer in a duct. The wall region of the duct was treated inviscidly and the duct wall was turned to generate shock and expansion waves. All calculations were performed using the $k\epsilon 1$ turbulence model[6] and employed 30 grid points equally spaced between the duct walls.

Waves Generated by Supersonic Shear Layer

In the first calculation, the duct walls remained parallel. Exhibited in Fig. 1 are the perturbation pressure waves produced by the mixing of uniform Mach 2.4 and Mach 4.8 streams, both initially at $T=1000$ K and $P=1$ atm. As discussed in the Introduction, in high-speed mixing problems such as this, significant viscous (turbulent) dissipation occurs. This produces a peak temperature in the mixing layer and hence, a hot central region of lower density. Streamlines are diverted around this hot central region, producing compression waves. As the mixing layer grows, the extent of the hot central region increases and the pressure must increase correspondingly. This hot central zone has a local mass defect

Presented as part of Paper 83-0288 at the AIAA 21st Aerospace Sciences Meeting, Reno, Nev., Jan. 10-13, 1983; submitted Jan. 29, 1983; revision submitted Aug. 24, 1983.

*Technical Director, Propulsion Gas Dynamics Division. Member AIAA.

†Research Scientist, Propulsion Gas Dynamics Division. Member AIAA.

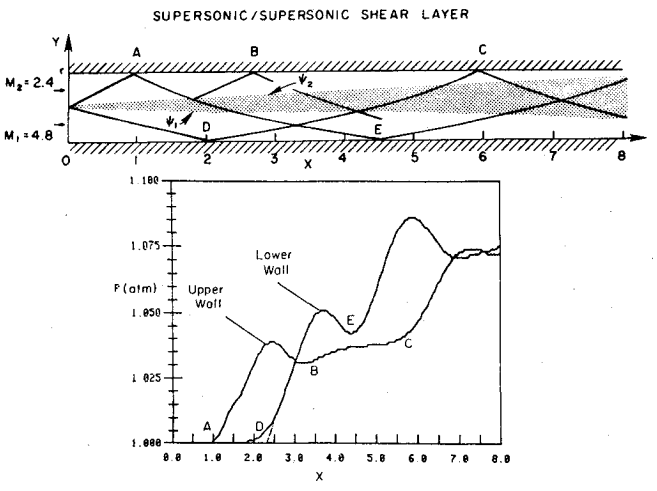

Fig. 1 Waves generated by supersonic shear layer; pressure variations along duct walls.

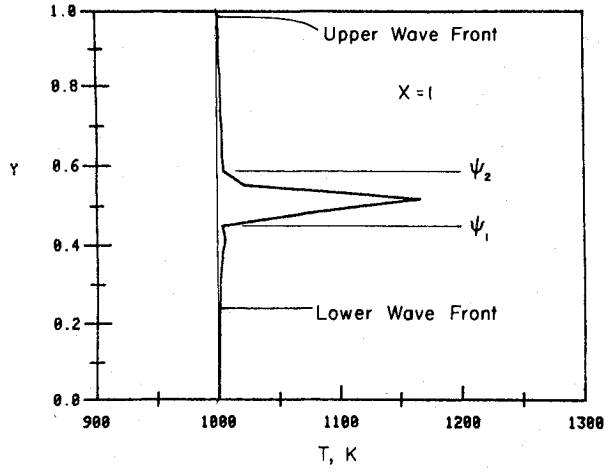

Fig. 2 Temperature profile at $x = 1$ exhibiting extent of shear layer and wave fronts.

producing a positive displacement effect akin to that of a boundary layer. The displacement thickness increases with the growth of the mixing region. In supersonic combustion problems,[7] or in situations with larger velocity ratios or higher Mach numbers, the heat produced will be much greater and shock waves will be generated.

The initial wave fronts are clearly displayed in the temperature profile at $x = 1$ (Fig. 2), which shows a sharp distinction between the mixing region and the perturbed outer flow. The wave fronts in the initial region ($0 < x < 2$) are also readily displayed by the normal velocity profiles depicted in Fig. 3. Inspection of the profiles indicates that the normal velocity is essentially zero in the center of the mixing layer, positive above this point, and negative below it. Hence, the streamlines are seen to be diverted about this central point where the temperature peaks. Note that maximum and minimum values of the normal velocity occur near the edges of the mixing layer. Outside the mixing layer, the streamlines are deflected due to the mixing induced compression systems. Consider the profile at $x = 0.5$. Peak maximum and minimum values occur at $y = 0.75$ and 0.3. At $x = 1$, the upper wave front has reached the wall while the lower wave front is at $y = 0.2$. At $x = 2$, the lower wave front has just reached the wall.

Temperature profiles are displayed in Fig. 4 at various axial stations. These profiles display the peak value in the center of the mixing layer and clearly distinguish the mixing layer and

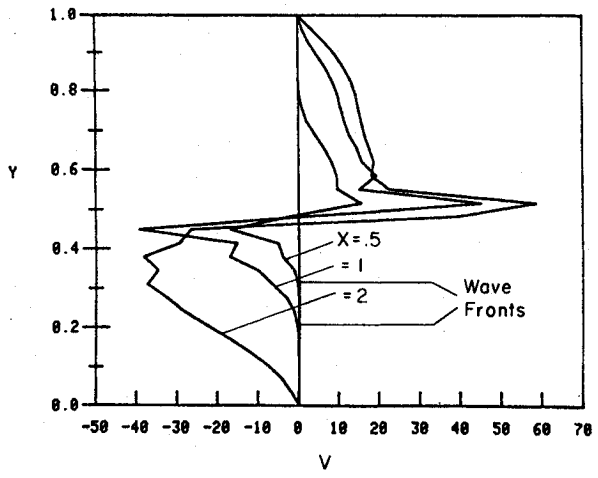

Fig. 3 Normal velocity profiles at several axial stations.

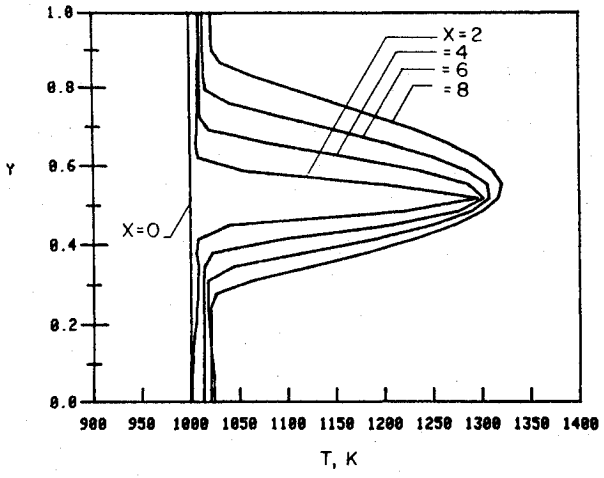

Fig. 4 Temperature profiles at several axial stations.

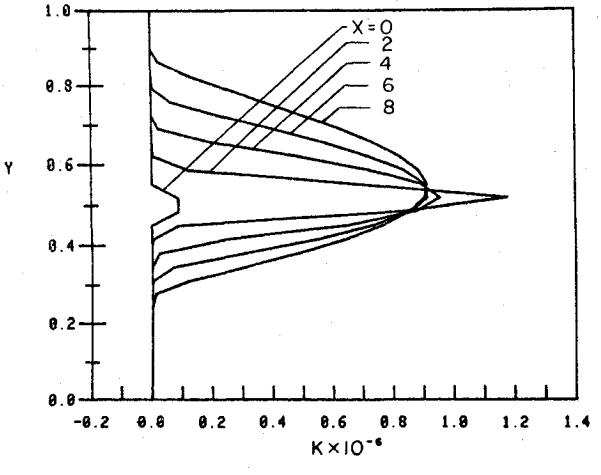

Fig. 5 Turbulent kinetic energy profiles at several axial stations.

wave zones. At $x = 2$, the temperature reaches the appropriate peak value of about 1300 K but the profile is sharp at the peak point and not yet fully developed. Here, only five grid points are within the mixing zone and thus the resolution is quite poor. The lower wave front is seen to reach the wall at this station. At $x = 4$, the profile starts to take on a rounded, fully developed appearance. The peak values at later stations go beyond 1300 K due to the continual compression waves in the flow.

Profiles of the turbulent kinetic energy are shown in Fig. 5. The initial level of k as given by a mixing length initialization is seen to be underestimated. Since the width of the initial mixing layer is quite small, this should have a negligible influence on the solution. The peak value of turbulent kinetic energy stabilizes at $x>4$. The profile at $x=2$ overshoots this value, indicating that the solution here is not yet fully developed. The peak value represents maximum velocity fluctuations of about 12.7%

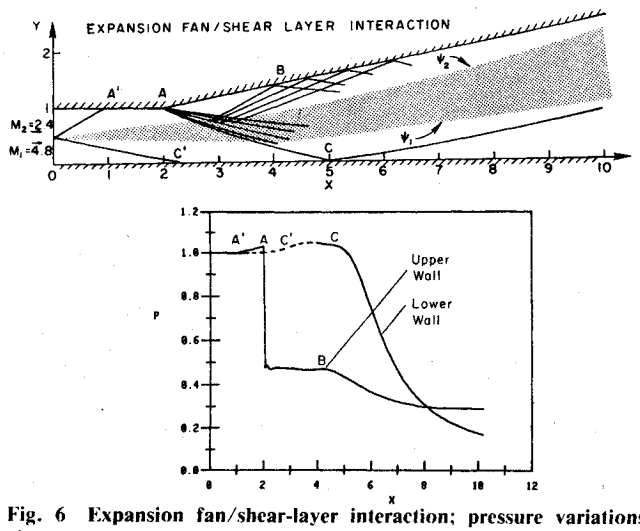

Fig. 6 Expansion fan/shear-layer interaction; pressure variations along duct walls.

The predictions indicate that the mean flow profiles do not become fully developed until $x>2$, while the turbulence profiles do not until $x>4$. This is due to lack of grid resolution in the shear layer. Use of the grid embedding procedure described in Part I[1] can be employed to remedy this deficiency.

Expansion Fan/Shear-Layer Interaction

This calculation has the same initial conditions and initial duct geometry as the previous case. At $x=2$, the upper wall is turned up by 0.2 rad generating a downrunning expansion fan that interacts with the shear layer. The interaction process involves the partial transmission of the expansion fan through the shear layer, the partial reflection of the fan from the shear layer, and, the alteration of mean flow and turbulence variables in the shear layer due to the expansion waves.

The predicted flow pattern and wall pressure variations are shown in Fig. 6. The pressure along the upper wall is perturbed at $x=1$ due to the mixing induced weak compressions and drops abruptly at the expansion corner ($x=2$) by a factor of about 2.3. The pressure then remains constant along the upper wall until the wave front of the reflected fan reaches the wall at $x\sim3.5$. At $x\sim8$, the interaction of the reflected fan with the upper wall appears completed. The pressure along the lower wall is perturbed at $x\sim2$ by the mixing induced compression with the front of the transmitted expansion wave reaching the lower wall at $x\sim5$.

The sequence of events is readily portrayed by inspection of the temperature profiles (Fig. 7) at various axial stations. At $x=2$, just downstream of the corner expansion, the wall

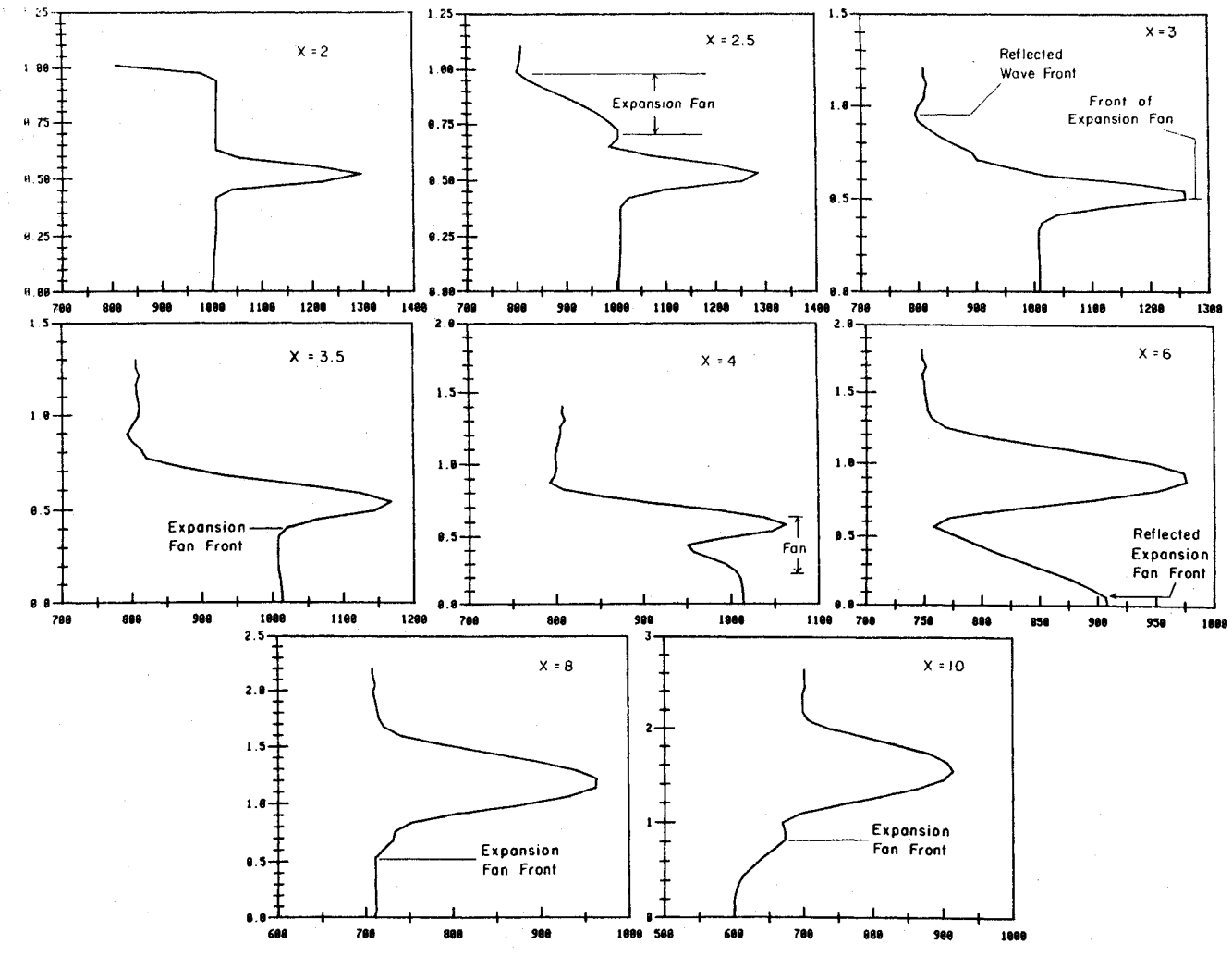

Fig. 7 Temperature profiles at various stations exhibiting the expansion fan interaction process.

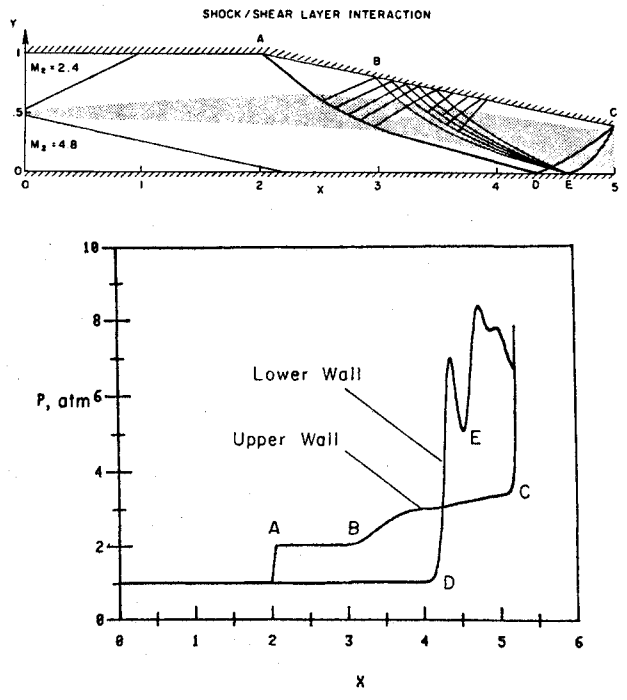

Fig. 8 Shock/shear-layer interaction; pressure variations along duct walls.

temperature decreases to 800 K behind the expansion fan. At $x=2.5$, the expansion fan is between $0.7<y<0.95$ and is about to intersect the shear layer. The reflected wave front is at $y\sim0.95$, but the strength of the initial reflected waves is quite small. At $x=3$, the front of the expansion fan has traversed half the shear layer and has reduced the peak temperature by about 50 K. At $x=3.5$, the front of the expansion fan has traversed the entire shear layer and the peak temperature is now 1175 K (reduced by 125 K). At $x=4.0$, the expansion fan is between $0.2<y<0.65$. Note that the peak temperature has dropped to 1060 K (by 240 K). The reflected waves generated in the interaction process are now starting to become appreciable as evidenced by temperature levels below 800 K at $y\sim0.8$-0.9. At $x=6$, the expansion fan front has reflected off the lower wall and is located at $y\sim0.1$. The peak temperature level has dropped to 975 K. Temperatures at the upper wall are now lowered to 750 K, resulting from the wave reflected from the shear layer. At $x=8$, the expansion fan front is at $y\sim0.5$, while at $x=10$ it is at $y\sim0.8$.

Shock/Shear-Layer Interaction

This calculation is analogous to that above with the upper wall turned down at $x=2$ by 0.2 rad. This generates a downrunning shock wave that interacts with the shear layer. The interaction process involves the partial transmission of the shock through the shear layer, the partial reflection of the shock from the shear layer, and the alteration of mean flow and turbulence variables in the shear layer due to the shock wave.

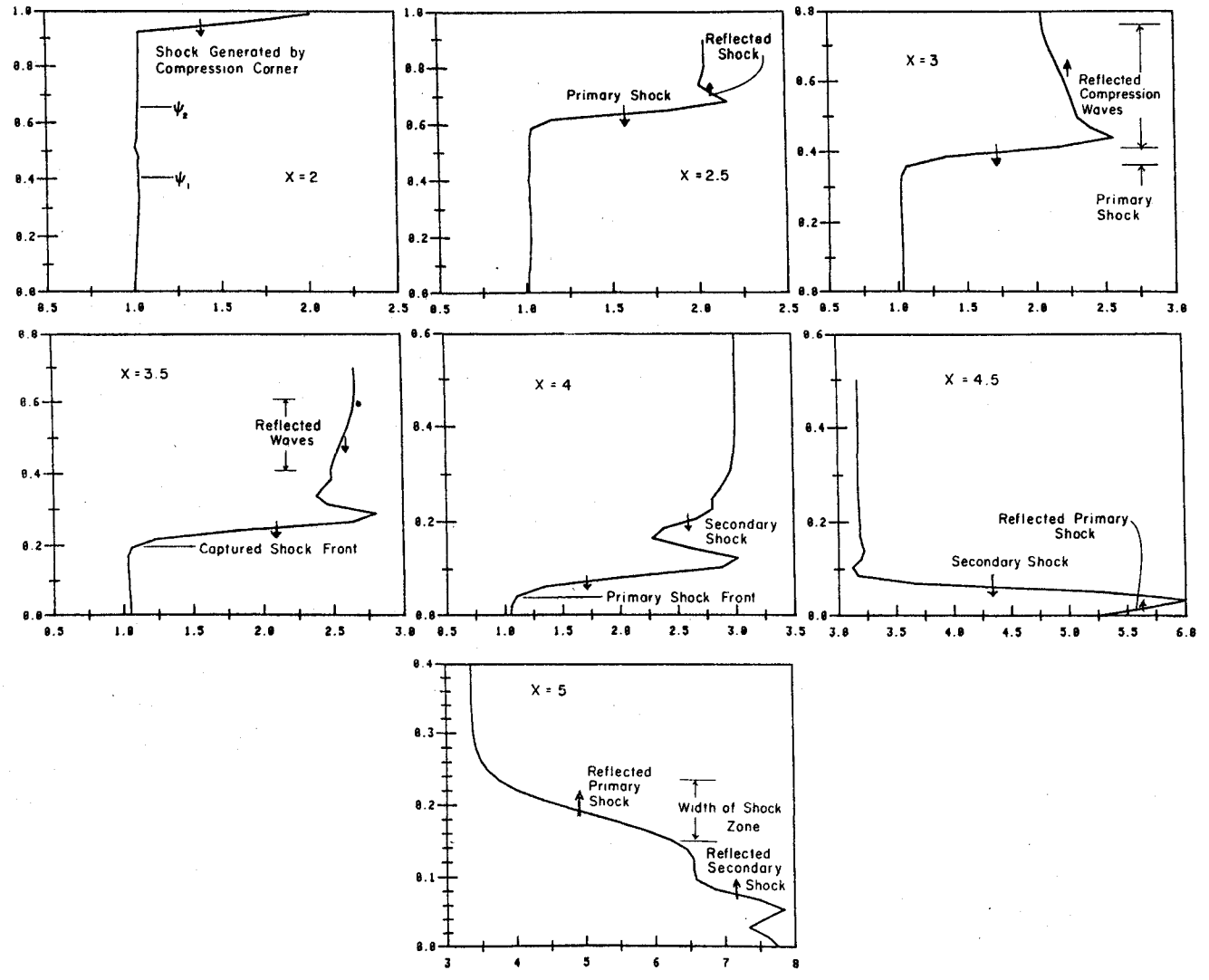

Fig. 9 Pressure profiles at various stations exhibiting the shock interaction process.

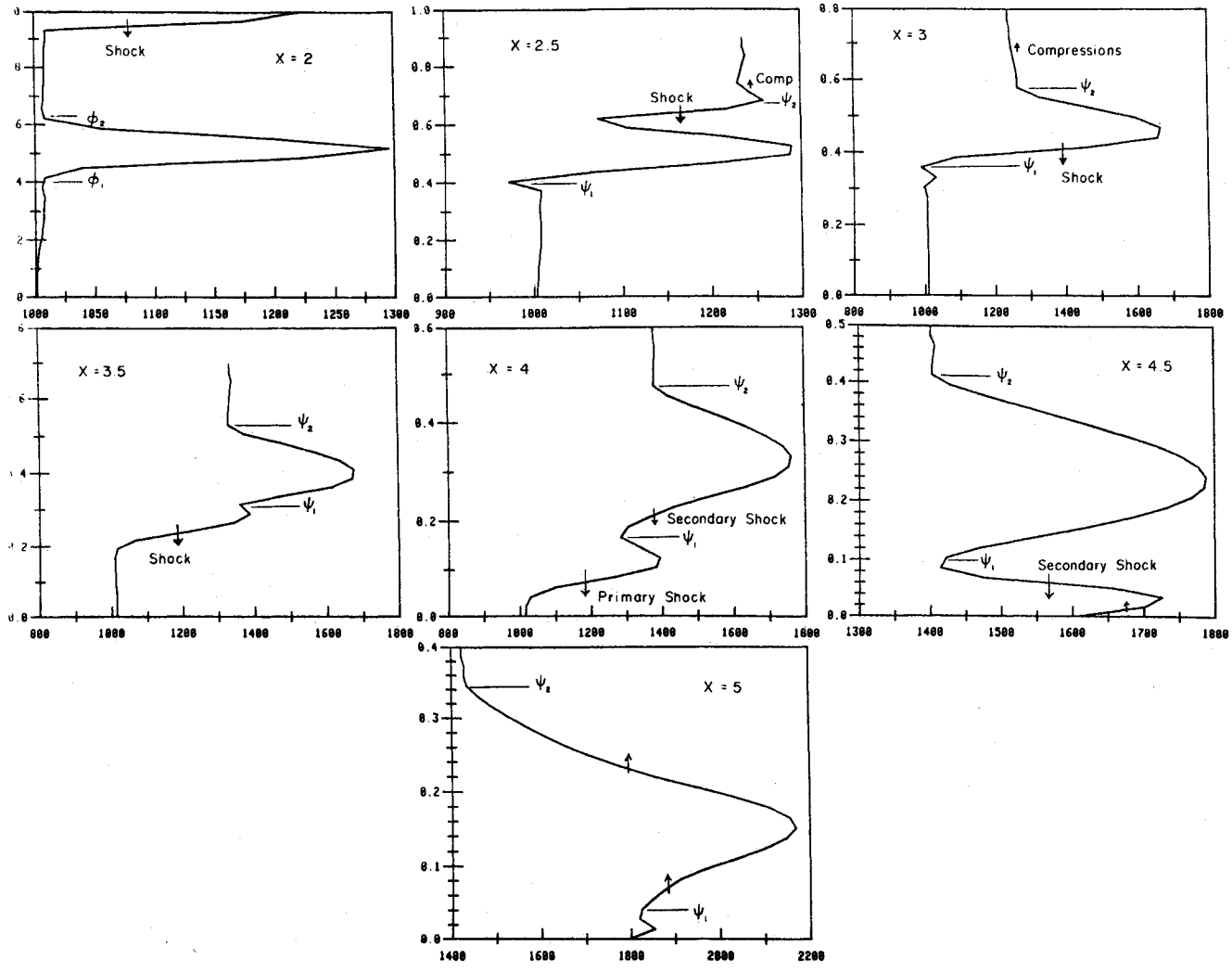

Fig. 10 Temperature profiles at various stations exhibiting the shock interaction process.

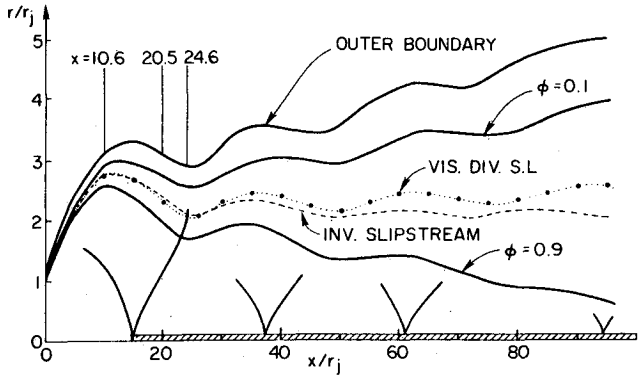

Fig. 11 Mach 3 jet into Mach 3 external stream; $P_j/P_e = 10$.

The predicted flow pattern and wall pressure variations are depicted in Fig. 8. The pressure perturbations induced by the initial mixing region are not distinguishable on this scale. The pressure along the upper wall increases by a factor of about 2 at the compression corner ($x=2$). It then remains constant until reflected compressions start impinging at $x\sim3$. The pressure along the lower wall remains constant until the downrunning shock generated at the compression corner impinges at $x\sim4.2$. The reflected compression waves generated by the interaction of the shock with the shear layer reflect from the upper wall as compressions and coalesce to form a shock in propagating to the lower wall. This second shock reaches the lower wall at $x\sim4.6$. The two shocks reflect off the lower wall and intersect in propagating back to the upper wall. They reach the upper wall at $x\sim5.2$, at which point the calculation is terminated since the flow behind this reflection point becomes subsonic.

This sequence of events is readily monitored by inspection of the pressure profiles at various axial stations (Fig. 9). At $x=2$, just downstream of the compression corner, the wall pressure is seen to have increased by a factor of 2. At $x=2.5$, the captured shock front has traversed about one-fourth of the shear layer. The interaction process is clearly displayed in this figure. The pressure level is seen to be constant ($P\sim2$) down-stream of the shock outside the shear layer but increases in the shear layer due to the reflected compression waves generated. At $x=3$, the shock has traversed the entire shear layer. The positions of the captured shock and the reflected compression waves are indicated. At $x=3.5$, the front of the captured shock is at $y\sim0.2$ and the compressions reflected from the upper wall are between $0.4<y<0.6$. At $x=4$, the primary shock is about to impinge on the lower wall while the compressions have focused to yield a secondary embedded shock located between $0.17<y<0.22$. At $x=4.5$, the primary shock has reflected, bringing the wall pressure to 5.25. The juncture of the downrunning secondary shock and uprunning reflected primary shock is at $y\sim0.025$ (where the pressure peaks at 6). At $x=5$, the reflected primary shock is between

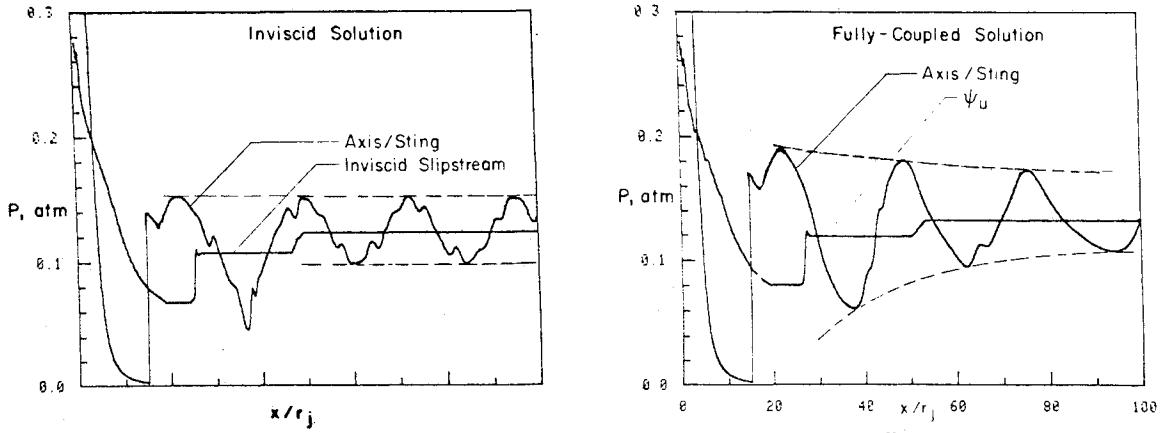

Fig. 12 Inviscid and fully coupled (PNS) pressure variations along jet centerline.

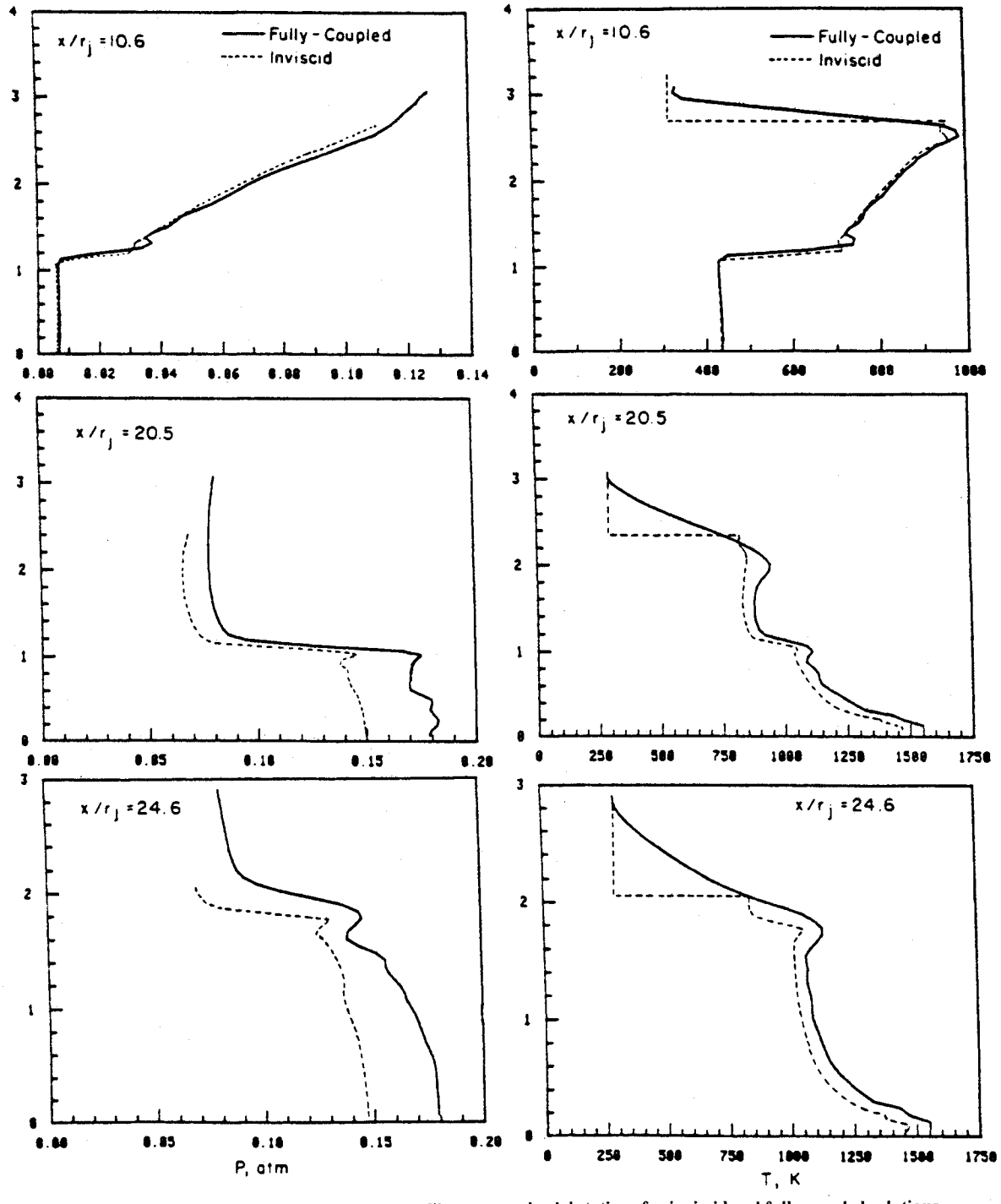

Fig. 13 Pressure and temperature profiles at several axial stations for inviscid and fully coupled solutions.

$0.15 < y < 0.24$ and is somewhat diffuse. The reflected secondary shock is between $0.05 < y < 0.1$.

These same events are portrayed in the temperature profiles given in Fig. 10. These profiles can be more informative than the pressure profiles since the shear layer region can be readily identified, which helps clarify interactive events. The shear-layer boundaries are labeled ψ_1 and ψ_2 in all the temperature profiles. Note that after the primary shock traverses the shear layer at $x=3$, the peak temperature increases to 1700 K.

After the secondary shock traverses at $x=4$, the temperature increases to about 1750 K. With the passage of the primary shock reflected from the lower wall at $x=5$, the temperature increases to 2150 K.

Further details of these fundamental interactive calculations are provided in Refs. 8 and 9.

Supersonic/Supersonic Jet Mixing

These calculations serve to exhibit the influence of the interactive phenomena occurring in the jet shear layer on the near-field jet shock structure. They were also performed using the $k\epsilon 1$ turbulence model.[6]

Mach 3 Jet/Mach 3 Stream

The first calculation simulates a Mach 3 jet exhausting into a Mach 3 external stream at a static pressure ratio of 10/1. The jet temperature was 1800 K and the external stream temperature was 300 K. The calculation was performed using a one-domain mapping extending from the axis to the outer mixing layer boundary. The inviscid supersonic external flow was represented by the use of pressure-flow deflection relations (see Ref. 10) applied at the outer boundary. The calculation was performed in both the fully coupled mode and in the inviscid limit. The predicted multiple-cell, fully coupled flow structure is exhibited in Fig. 11. A comparison of the viscous dividing streamline and inviscid slipstream shows them to be in very close proximity in the first inviscid cell and then to diverge beyond that point, with the viscous dividing streamline remaining above the inviscid slipstream. This would indicate that interactive effects are fairly weak in the first cell and then increase as the width of the mixing region becomes substantial. The axial pressure variations shown in Fig. 12 confirm this viewpoint. The inviscid and fully coupled Mach disk locations are essentially identical, with the fully-coupled solution having somewhat greater shock strengths, due to the additional compression waves generated by the displacement of streamlines about the hot central portion of the mixing layer. The inviscid solution exhibits a linear, nondecaying wave pattern beyond the first cell, while the fully coupled solution exhibits a nonlinear, decaying wave pattern.

Profiles of pressure/temperature (Fig. 13) at several stations in the first inviscid cell show the gradual buildup of viscous interactive effects. At $x/r_j = 10.6$, the two pressure distributions are nearly identical and the shear layer is quite thin. The temperature peaking due to viscous dissipation is not pronounced. At $x/r_j = 20.5$, the reflected shock is about to enter the plume mixing layer. The two reflected shock positions are nearly identical but the fully coupled solution has a stronger shock. At $x/r_j = 24.6$, the reflected shocks have reached the position of the viscous dividing slipstream or inviscid interface. This shock/shear-layer interaction is a strongly interactive phenomenon and, beyond this point, the two solutions start to noticeably diverge (see Fig. 11). Up until this point, the use of overlaid weakly interactive coupling[11] would be valid. However, for situations with stronger near-field interactions, as induced by faster mixing or chemistry, the overlaid approximation inadequately represents the plume near field.

Mach 5 Jet/Mach 2 Stream

To demonstrate this latter point, the calculation was modified by increasing the jet velocity and decreasing the external stream velocity, keeping all other conditions the same. Here, the jet Mach number is boosted to 5 and the external Mach number is decreased to 2. The nominal velocity ratio has been increased from about 2½/1 to about 7/1. The predicted flow structure is shown in Fig. 14. The near-field interactions are shown to be quite pronounced, with the viscous dividing streamline and inviscid slipstream positions departing just beyond the nose region of the plume. The near-field positive displacement effect significantly strengthens the barrel shock, resulting in a fully coupled Mach disk position well upstream of the inviscid disk position, as indicated by the axis pressure variation curves in Fig. 15 (the fully coupled disk position is at $x/r_j \sim 27$, while the inviscid disk position is at $x/r_j \sim 35$). The subsequent fully coupled shock locations and cell lengths are considerably foreshortened in comparison to the inviscid solution due to the substantial curvature of the shocks in traversing the highly rotational mixing layer. The shock structure here is significantly stronger than that of the previous Mach 3/Mach 3 case (note that the pressures are now plotted on a log scale) since the impinging shock waves are largely reflected from the shear layer due to the higher vorticity. In the previous case, the ratio of reflected to transmitted wave strengths is much lower.

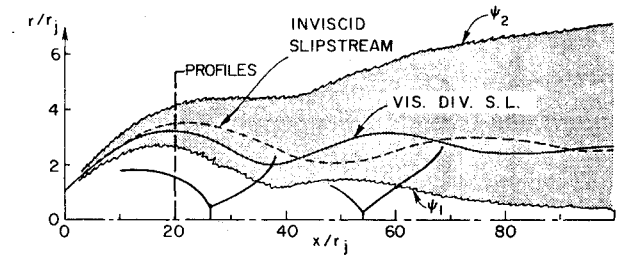

Fig. 14 Mach 5 jet into Mach 3 external stream; $P_j/P_e = 10$.

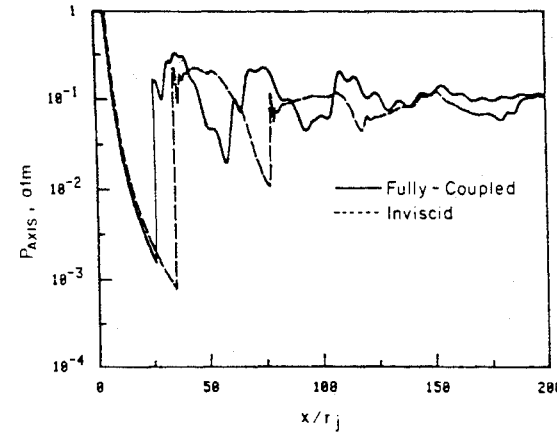

Fig. 15 Comparison of inviscid and fully coupled jet centerline pressure variations.

Profiles at $x/r_j = 20$ shown in Fig. 16 exhibit the magnitude of the near-field interactive effects. The shock propagation patterns as evidenced by the pressure and temperature profiles are quite different. The fully coupled barrel shock propagates much faster and is at $r/r_j \sim 1.5$ while the inviscid shock is at $r/r_j \sim 2$. The cause of the significant displacement effect is quite evident: the viscous temperature peak is about 1500 K above the inviscid temperature. This is caused by the very high shear and very high Mach numbers in this case. The same interactive effects would occur at more realistic velocity ratios and Mach numbers in cases with significant after-burning.

Supersonic/Subsonic Jet Mixing

Mildly Underexpanded Mach 2 Jet

This calculation simulates the experiment of Seiner and Norum[2,3] for a cold ($T = 164$ K) Mach 2 jet into still air at a

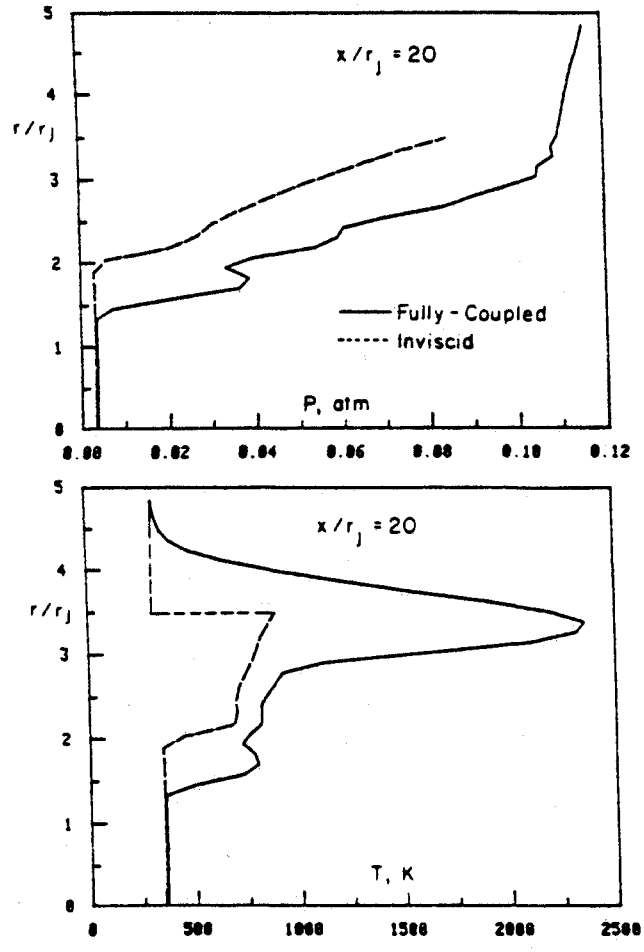

Fig. 16 Comparison of pressure and temperature profiles at $x/r_j = 20$.

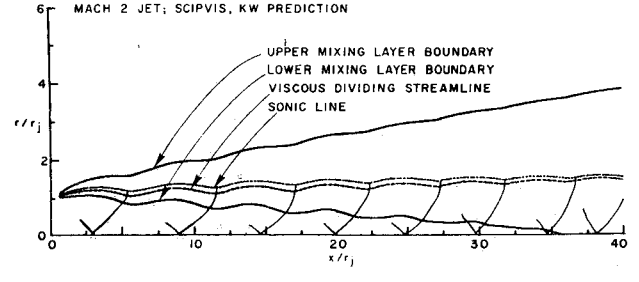

Fig. 17 Mach 2 jet into still air; $P_j/P_e = 1.445$.

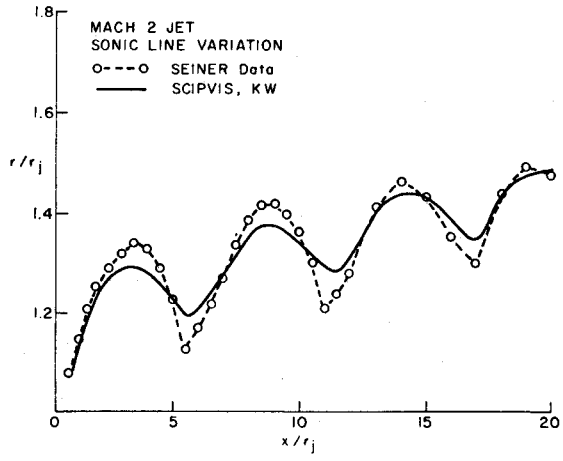

Fig. 18 Comparison of predicted shear layer sonic line variation with data; kW turbulence model.

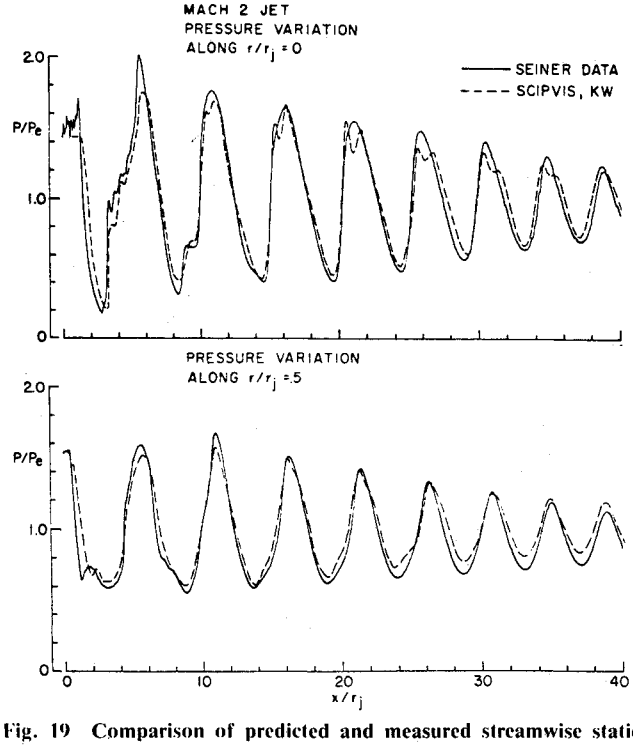

Fig. 19 Comparison of predicted and measured streamwise static pressure variations along jet axis and radial position $r/r_j = 0.5$.

static pressure ratio (P_j/P_E) of 1.45/1. The predicted flow structure for this case (using the kW turbulence model[12]) is exhibited in Fig. 17 for the first 40 jet radii in which eight shock cells occur. The nominal upper and lower mixing layer boundaries (where $\phi = 0.05$ and 0.95, respectively), the jet mixing layer sonic line, and the viscous dividing stream (where $\psi = \psi_j$) are all depicted. Note that the mixing layer engulfs the entire jet downstream of $x/r_j \sim 35$. The sonic line initially sits above the viscous dividing streamline, intersects it at $x/r_j \sim 45$, and ultimately reaches the axis. The details of the predicted sonic line variation for the first four shocks (Fig. 18) are shown to agree quite well with the measurements.

Comparisons of the predicted and measured streamwise pressure variations along the jet centerline and along $r/r_j = 0.5$ are exhibited in Fig. 19. The comparison is seen to be quite good, indicating that the growth of the mixing region (which controls the variation of the sonic line and hence the shock cell spacing) and the attenuation of wave intensities by turbulent dissipation are both properly modeled. A comparison of predicted (using the kW model) and measured[2,3] longitudinal turbulent intensities is given in Fig. 20 along the jet lipline ($r/r_j = 1$). Both the measured and predicted variations indicate that the turbulence levels peak at the end of compression zones and are minimum at the end of expansion zones. The comparison is quite encouraging in that the levels predicted based on peak ($\overline{u'u'} = 2k$) and isotropic ($u'u' = 2k/3$) estimates of the longitudinal intensity bound the measurements (see the discussion in Ref. 4).

In performing these calculations, a small, nonzero value of the streamwise edge velocity was assigned, and the external pressure was set equal to the ambient value at all grid points above the sonic line. This represents a *first approximation* to the overall interactive solution which adequately represents the flow structure in the first 8-10 shock cells. Beyond this region, the influence of the external stream velocity and pressure variations induced by the accelerative effects of jet entrainment influence the flow structure. (See the sensitivity studies of Seiner et al.[4] exhibiting the influence of the small

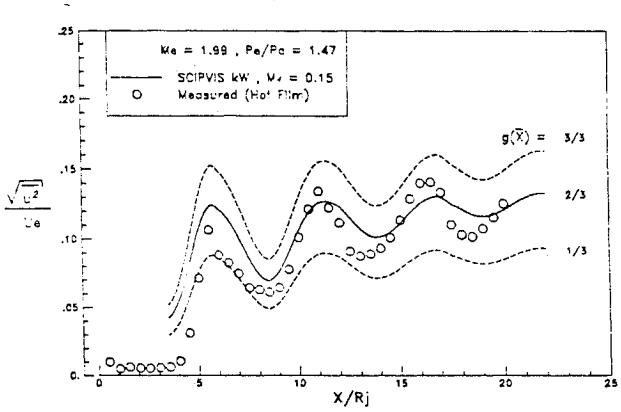

Fig. 20 Streamwise variation of longitudinal turbulent intensity along jet lip line; $u'^2 = 2gk$.

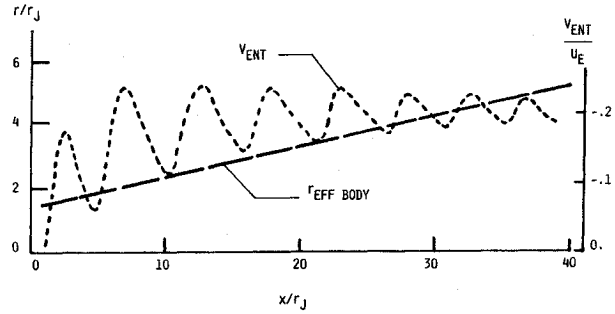

Fig. 21 Effective geometric matching surface ($r_{EFF\ BODY}$) for direct jet/potential flow coupling and variation of entrainment velocity (V_{ENT}) along matching surface.

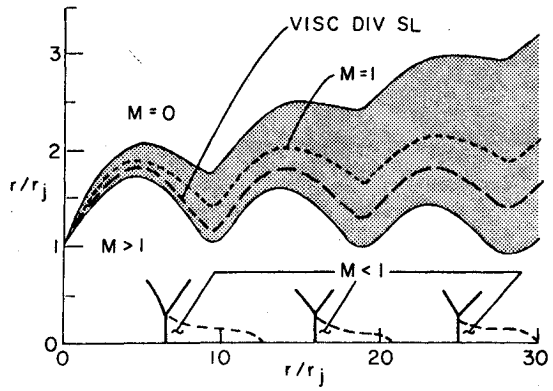

Fig. 22 Mach 2 jet into still air; $P_j/P_e = 3$.

external stream velocity.) To account for these effects, direct coupling with a potential flow solver[13,14] is required. Here, the external flow pressure and velocity perturbations induced by jet entrainment are obtained by solving the potential flow about a geometric body whose surface corresponds to the "mean" outer mixing layer edge and along which the source distribution is prescribed in accordance with the predicted entrainment (radial) velocity distribution. The effective geometric body and predicted entrainment velocity distribution for this case are exhibited in Fig. 21. The resultant pressure and streamwise velocity variations obtained from the potential flow solution are then imposed as outer edge conditions for a revised jet calculation, and several jet/potential flow iterations are performed until a converged solution is arrived at.

Moderately Underexpanded Mach 2 Jet

To exhibit the treatment of small, embedded subsonic regions behind Mach disks, the calculation above was

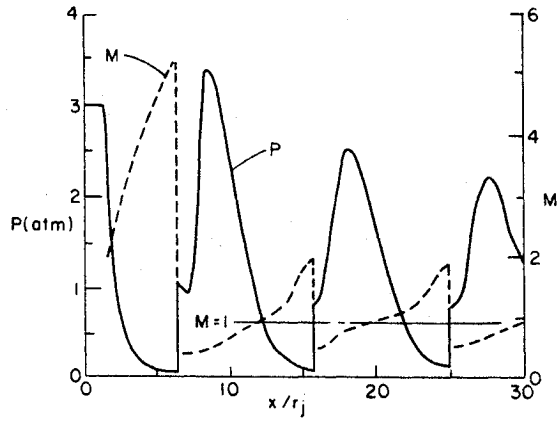

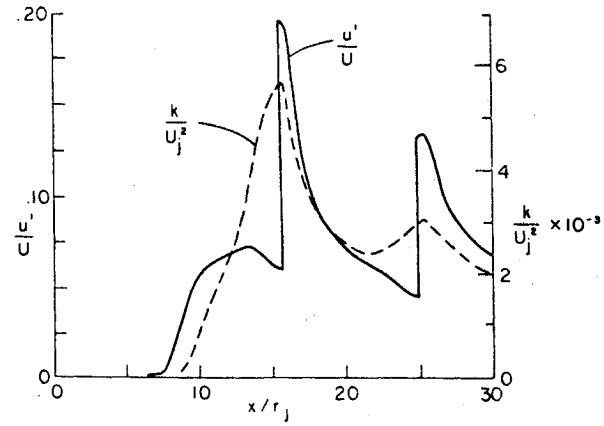

Fig. 23 Variation of pressure, Mach number, turbulent kinetic energy, and turbulent intensity along jet centerline.

repeated with the exit static pressure ratio boosted to 3/1. The previous case had no Mach disks (regular reflection of the shocks at the axis occurred). The predicted flow structure for three shock cells using the kW turbulence model is exhibited in Fig. 22. A highly expanded radial scale is utilized to show some details of the embedded subsonic domains behind the Mach disks. These domains are seen to be quite small for the small radius Mach disks in this case. The variation of pressure, Mach number, turbulent kinetic energy, and scaled turbulent intensity [i.e., u'/U where $u' \sim (2k/3)^{1/2}$] along the jet centerline are exhibited in Fig. 23. The subsonic region is seen to extend about 5 jet radii beyond each disk (corresponding to about 15 Mach disk radii). The mixing process is quite rapid and remains confined to the region of the jet centerline. The scaled turbulent intensities increase abruptly behind the second and third disks due to the abrupt decrease in the streamwise velocity in crossing the Mach disk. The turbulent kinetic energy peaks in the vicinity of the second Mach disk and then rapidly diminishes, peaking slightly in the vicinity of the third disk position. The shape of the sonic line and the overall characteristics of the Mach disk mixing process are in qualitative accord with the experimental observations of Back and Cuffel.[15]

Concluding Remarks

Numerical studies presented herein serve to portray the types of interactive phenomena one may encounter in supersonic jet mixing problems. The ability of the numerical modeling techniques discussed in Part I[1] to calculate these phenomena was exhibited both qualitatively and quantitatively. This preliminary study has served to demonstrate the overall viability of the approach taken. A number of computer models are now under development which utilize this approach to address various jet related problems.

The SCIPVIS model[5,9] has been developed to analyze the detailed, multiple-cell shock structure in imperfectly expanded, axisymmetric free jets for utilization in the prediction of jet shock noise.[4] This developmental effort has provided us with the opportunity to explore the sensitivity of the jet flowfield solution to the turbulence modeling employed. This topic is too lengthy to be included herein; it is discussed in detail in Refs. 5 and 9. It is shown that present generation "compressibility-corrected" two-equation turbulence models can reasonably represent the turbulence processes occurring in simple (nonreacting, single-phase) imperfectly expanded jets. This viewpoint is fortified by comparisons of SCIPVIS predictions with the data of Seiner and Norum[2,3] for a number of imperfectly expanded, sonic, Mach 1.5 and Mach 2 jets exhausting into still air. This assessment study is documented in Ref. 4. Experiments are now in progress by Seiner at NASA/LRC for free jets exhausting into supersonic external streams and SCIPVIS will be utilized to analyze these new data. An extended version of SCIPVIS has been developed to analyze jets with plug centerbodies and the data of Kibens and Wlezien[16] are now being analyzed.

This approach has been extended to analyze axisymmetric rocket exhaust plumes, involving the additional consideration of nonequilibrium chemistry and two-phase flow processes. Progress in this model development effort is described in Refs. 17 and 18. This approach has also been extended to calculate three-dimensional jet flowfields,[19] and preliminary calculations have been performed for jets exhausting from rectangular nozzles.

Acknowledgments

This work was supported by the Propulsion Aerodynamics and Aeroacoustics Branches of the NASA Langley Research Center under Contract NAS1-16535. The cognizant technical monitors were Dr. R.G. Wilmoth, Propulsion Aerodynamics Branch, and Dr. J.M. Seiner, Aeroacoustics Branch.

References

[1] Dash, S.M. and Wolf, D.E., "Interactive Phenomena in Supersonic Jet Mixing Problems, Part I: Phenomenology and Numerical Modeling Techniques," *AIAA Journal*, Vol. 22, July 1984, pp. 905-913.

[2] Seiner, J.M. and Norum, T.D., "Experiments of Shock Associated Noise on Supersonic Jets," AIAA Paper 79-1526, July 1979.

[3] Seiner, J.M. and Norum, T.D., "Aerodynamic Aspects of Shock Containing Jet Plumes," AIAA Paper 80-0965, June 1980.

[4] Seiner, J.M., Dash, S.M., and Wolf, D.E., "Shock Noise Features Using the SCIPVIS Code," AIAA Paper 83-0705, April 1983.

[5] Dash, S.M. and Wolf, D.E., "Shock-Capturing Parabolized Navier-Stokes Model (SCIPVIS) for the Analysis of Turbulent Underexpanded Jets," AIAA Paper 83-0704, April 1983.

[6] Launder, B.E., Morse, A., Spalding, D.B., and Rodi, W., "Prediction of Free Shear Flows: A Comparison of Six Turbulence Models," *Free Turbulent Shear Flows*, Vol. I, NASA SP-321, 1972, pp. 361-426.

[7] Ferri, A., "Mixing-Controlled Supersonic Combustion," *Annual Review of Fluid Mechanics*, Vol. 5, 1973, pp. 301-338.

[8] Dash, S.M. and Wolf, D.E., "Development of Fully-Coupled Viscous/Inviscid Technology for the Analysis of Exhaust Plume Flowfields," *Proceedings of JANNAF 13th Plume Technology Meeting*, CPIA Pub. 357, Vol. I, April 1983, pp. 115-183.

[9] Dash, S.M. and Wolf, D.E., "Fully-Coupled Analysis of Jet Mixing Problems, Part I: Shock-Capturing Model, SCIPVIS," NASA CR 3761, Jan. 1984.

[10] Dash, S.M. and Thorpe, R.D., "Shock-Capturing Model for One- and Two-Phase Supersonic Exhaust Flow," *AIAA Journal*, Vol. 19, July 1981, pp. 842-851.

[11] Dash, S.M., Wilmoth, R.G., and Pergament, H.S., "An Overlaid Viscous/Inviscid Model for the Prediction of Nearfield Jet Entrainment," *AIAA Journal*, Vol. 17, Sept. 1979, pp. 950-958.

[12] Jensen, D.E. and Wilson, A.S., "Prediction of Rocket Exhaust Flame Properties," *Combustion and Flame*, Vol. 25, 1975, pp. 43-55.

[13] Dash, S.M., Beddini, R.A., Wolf, D.E., and Sinha, N., "Viscous/Inviscid Analysis of Curved Sub- or Supersonic Wall Jets," AIAA Paper 83-1679, July 1983.

[14] Dash, S.M., Pergament, H.S., and Wolf, D.E., "Computation of Viscous/Inviscid Interactions in Exhaust Plume Flowfields, Part I: Overlaid and Fully-Coupled Methodology," *Proceedings of the Symposium on Rocket/Plume Fluid Dynamic Interactions*, Vol. I, ARO Fluid Dynamics Lab., Rept. 83-101, April 1983.

[15] Back, L.H. and Cuffel, R.B., "Viscous Slipstream Flow Downstream of a Centerline Mach Reflection," *AIAA Journal*, Vol. 9, Oct. 1971, pp. 2017-2019.

[16] Kibens, V. and Wlezien, R.W., "Porous-Plug Flowfield Mechanisms for Reducing Supersonic Jet Noise," AIAA Paper 83-0774, April 1983.

[17] Dash, S.M., Beddini, R.A., Wolf, D.E., and Pergament, H.S., "Analysis of Two-Phase Flow Processes in Rocket Exhaust Plumes," AIAA Paper 83-0248, Jan. 1983.

[18] Dash, S.M., Wolf, D.E., and Pergament, H.S., "Overlaid and Fully-Coupled Two-Phase Flow Versions of JANNAF Standard Plume Flowfield Model," *Proceedings of JANNAF 14th Plume Technology Meeting*, CPIA Pub. 384, Vol. II, Nov. 1983, pp. 169-226.

[19] Dash, S. M., Wolf, D. E., and Sinha, N., "Parabolized Navier-Stokes Analysis of Three-Dimensional Supersonic and Subsonic Jet Mixing Problems, AIAA Paper 84-1525, June 1984.